Int. J. Electrochem. Sci., 13 **(2018)** 9374 – 9384, doi: 10.20964/2018.10.55

International Journal of ELECTROCHEMICAL SCIENCE
www.electrochemsci.org

An Oxygen Sensor based on Electrospun Carbon Nanofibers Modified with Pd Particles

Yu-Ching Weng[1,*], *Zhao-Nan Wang*[1], *Shu-Yii Wu*[1,2]

[1] Department of Chemical Engineering, Feng Chia University, Taichung 40724, Taiwan
[2] Green Energy Development Center, Feng Chia University, Taichung 40724, Taiwan
[*]E-mail: ycwneg@fcu.edu.tw

Received: 16 June 2018 / *Accepted:* 3 August 2018 / *Published:* 1 September 2018

Electrospun carbon nanofibers modified with Pd sensors have been developed for O_2 sensing with high sensitivity. The average diameter of carbon nanofiber and Pd particle is about 251 and 20.5 nm, respectively. The sensing performances of the Pd decorated carbon nanofiber (Pd-CNF) electrode towards reduction of O_2 were evaluated. The Pd-CNF electrode with a Pd loading of 4.7 mg/cm^2 shows maximum sensitivity of 2.6 μAppm^{-1}cm^{-2} in the O_2 concentration region of 100-1000 ppm. The response and recovery times are less than 32 and 48 s, respectively. The high sensitivity, wide linear range and rapid response and recovery times make the Pd-CNF electrode a promising candidate for amperometric O_2 sensors.

Keywords: Pd, CNF, sensor, oxygen, electrospinning

1. INTRODUCTION

Detection of environmental oxygen content is important in various fields including the medicine, aquaculture, farming, chemical industries, fuel combustion and military [1-2, 24-26]. The ambient oxygen concentration is also considered to be a safety factor for industrial applications. Electrochemical gas sensors are the most promising among all the possible replacements because of their compact structure, low cost and the ability to monitor continuously [3]. Based on the working signal produced by the electrochemical cell, electrochemical gas sensors can be divided in two main categories of sensors including amperometric and potentiometric sensors. Amperometric sensors with linear relationship of the current response have received great attention due to their high sensitivity, wide detection range and short response time [4-5]. It has been reported that Pt, Pd and Au can be used as materials for amperometric oxygen sensors [6-8].

Electrospinning is a manufacturing process that can produce ultra fine fibers with diameter ranging from 50 to 500 μm [9]. Nanofibers fabricated via electrospun possess much higher specific surface and relatively larger porosity than flat films, making them excellent candidates for potential applications in sensors. Carbon nanofibers (CNFs) are good supporting material for catalytic metal particles (NPs). Many types of metal NPs, such as Pt , Pd, Au , Ag, Co and Cu have been assembled on carbon nanomaterials by using different methods [10]. Smaller particle morphology gives a better sensing capability as surface area and active reaction sites increase [11-12]. The metal NP/CNF nanocomposites have shown great promises in sensing applications [13]. Pd NPs are widely used for O_2 reduction in fuel cell applications [14-15]. CNFs used as supports to disperse Pd NPs could enhance their catalytic efficiency. This paper describes the application of the Pd decorated electrospun carbon nanofiber electrode as an amperometric sensor for oxygen determination.

In this work, a novel Pd decorated carbon nanofiber electrode was successfully prepared by a two step procedure which consists of electrospinning and chemical reduction method. Field-emission scanning electron microscopy (FE-SEM) and X-ray photoelectron spectroscopy (XPS) were applied to investigate the morphology and chemical state of the as-prepared sample. The Pd decorated carbon nanofiber electrode exhibits good morphological and structural stability at room temperature and shows high sensitive, reversible and fast response towards O_2.

2. EXPERIMENTAL SECTION

2.1 Preparation of CNFs

Polyacrylonitrile (PAN) with molecular weight of 150000 g/mol purchased from the Scientific Polymer Products, Inc. was used as a carbon source. *N, N*-dimethylformamide (DMF) was adopted as a solvent. In order to prepare a homogenous PAN solution, 8 wt% PAN powders were added to a DMF solvent and vigorously stirred for 12 hours. The polymer solution was pour into the spinning tank for electrospun. Electrospinning was performed using a homemade needless system. The elecrospinning process was carried out under the following conditions: 30° C temperature, 50% humidity, 50 kV supplied voltage and 15 cm working distance. The PAN nanofibers were then dried in oven for 24 hours to ensure that the solvent was completely evaporated. The stabilization of the PAN nanofibers was carried out in air by heating up to 320^{o}C temperature at a heating rate of 1^{o}C/min, and sample was kept at 320^{o}C for 1 hr. Carbonization process of the stabilized PAN nanofibers was carried out under a nitrogen flow at 900^{o}C for 1 hr at a heating rate of 5^{o}C/min in a tube furnace. The carbon nanofibers (CNFs) were then obtained.

2.2 Preparation of the Pd-CNF electrode

$PdCl_2$ (0.1 mol), CNFs (0.1 g) and distilled water (10 ml) were loaded into a three-necked flask while stirring. The mixture was heated to 70^{o}C and kept at this temperature for 20 min, after which methanol (20 ml) was injected into the solution. The mixture was incubated at 70^{o}C for 5 h. After

cooling down to the room temperature, the black precipitate was centrifuged and washed several times with distilled water. The Pd-CNFs (0.1 mg) were the mixed with Nafion solution (0.6 mg, 5 wt%) and distilled water (0.6 mg) by ultrasonic for 20 min. The obtained suspension (100 μl) was deposited on the Nafion membrane. The sample was then placed in a hot-press and heated at 135^{o}C with 25 kg/cm^{2} for 90 s. The resulting Pd-CNF electrode was stored in air at room temperature before use.

2.3 Characteristics of the Pd-CNF electrode

The surface morphology was examined by means of a Hitachi S-2500 FESEM with an accelerating voltage of 20 kV. The chemical states of the surface were studied by XPS measurements conducted on a Phi5000 spectroscope (ESCA system, Ulvac-Phi Co.) using a monochromated Al Kα X-ray source (1486.6 eV) operating at 15 kV. The electrochemical measurements were performed on a potentiostat/galvanostat (Model VersaSTAT 3, AMETEK Scientific Instruments, USA) with a typical three-electrode system composed of a platinum foil as counter electrode, an Ag/AgCl/KCl (sat.) in aqueous solution as reference electrode and the Pd-CNF electrode as working electrode. Nafion membrane not only played as a substrate but also a separator to divide the electrochemical cell into a gas chamber and a liquid chamber. Cyclic voltammograms (CVs) were carried out in a quiescent solution. Amperometric experiments were performed in a continuous stirring 0.5 M $HClO_4$ aqueous solution using a magnetic stirrer. In the case of O_2 experiments, the electrolyte solution was deoxygenated by passing through highly pure nitrogen for 10 min. A flow of nitrogen was maintained over the solution during experiments.

3. RESULTS AND DISCUSSION

3.1 Morphology and Chemical States of the Pd-CNFs

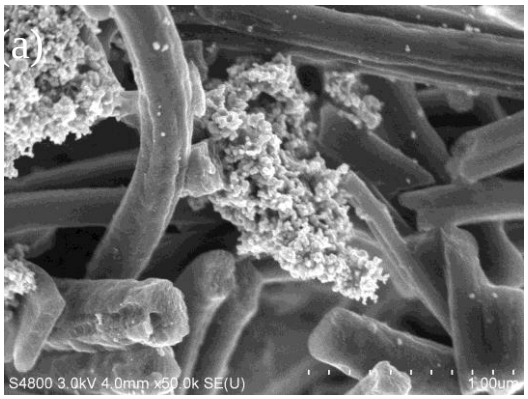

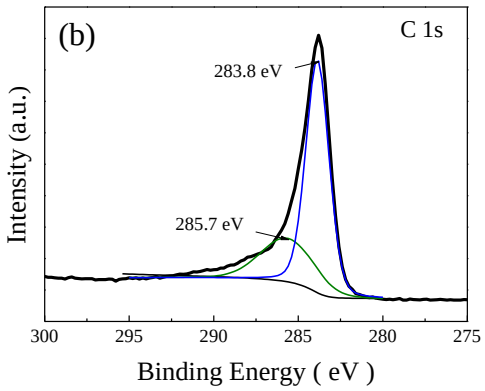

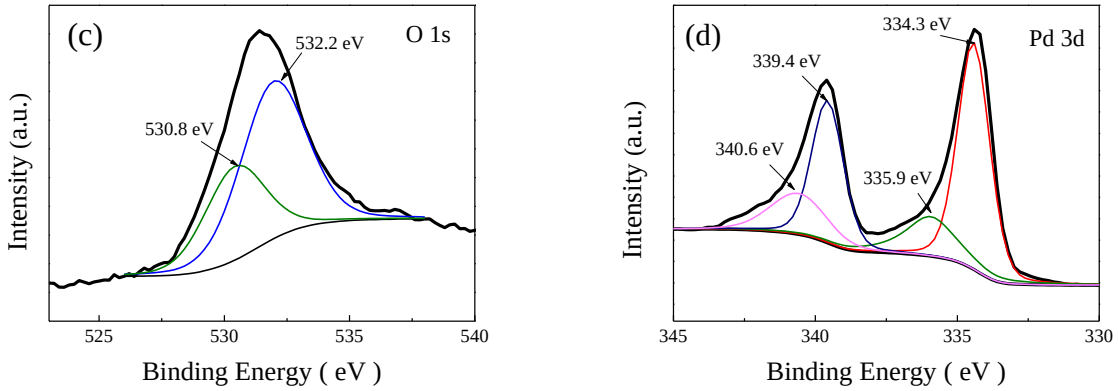

Figure 1. SEM image of surface morphology of Pd-CNF (a), XPS spectra of Pd-CNF corresponding to (b) C 1s (c) O 1s and (d) Pd 3d.

The surface morphology of the electropun Pd-CNFs by SEM is shown in Fig. 1(a). The CNFs are randomly oriented while the Pd nanoparticles are filled in the interstices of CNFs. The averages diameter of CNF and Pd nanoparticles is approximately 251 and 20.5 nm, respectively. X-ray photoelectron spectroscopy (XPS) measurements were used to elucidate the chemical binding energy state of the Pd-CNF electrode and results are shown in Fig. 1(b-c). All spectra are calibrated using the C 1s peak of carbon present at 284.2 eV. Fig. 1(b) shows the C 1s spectrum, which is fitted into two individual component peaks at binding energy (BE) of 283.8 and 285.7 eV, respectively. These peaks represent graphite carbon with C-C and C-O-C bonds [16]. The O 1s spectrum is shown in Fig. 1(c). The broad peaks for O 1s are asymmetric and can be fitted as two peaks. The peak at about 530.8 eV and the relative higher BE peak at 532.2 eV may be assigned to C=O and C-OH [16]. The Pd 3d spectrum can be deconvoluted into two pairs of doublets as shown in Fig. 1(d). The binding energies of 334.3 and 339.4 eV are respectively ascribed to Pd 3d5/2 and Pd 3d3/2, which indicates the presence of metallic Pd [10]. The higher binding energies at 335.9 and 340.6 eV are attributed to Pd^{2+}, which could be PdO [17]. The ratio of the areas under the curves for Pd and Pd^{2+} is approximately 68:33 for the Pd-CNF electrode.

3.2 Cyclic Voltammograms of the CNF and Pd-CNF Electrodes in the Absence and Presence of Oxygen

Figure 2 shows cyclic voltammograms of the CNF and Pd-CNF electrodes in 0.5 M $HClO_4$ solutions with and without 1000 ppm oxygen. No obvious redox peaks can be observed on CNF electrode indicating CNF is stable in the selected potential region without any redox reaction. However, the CNF electrode displays very low electrocatalytic activity for oxygen reduction. In the absence of oxygen, the Pd-CNF electrode exhibits a typical behavior of Pd metal and presents a peak between 0.28 and 0.3 V, corresponding to hydrogen adsorption and desorption. The region between 0.3 and 0.53 V indicates a clean Pd surface in the Pd-CNF electrode. We also found the formation of Pd oxides when scanned potential is above 0.53V. The oxygen reduction peak on the Pd-CNF electrode appeared at 0.4V on the reverse scan. The reduction current increased with a negative potential from 0 to -0.4V.

The remarkable electrocatalytic activity of Pd-CNF toward the reduction of oxygen may be attributed to the distribution of Pd nanoparticles in CNF matrix may provide large catalytic surface area.

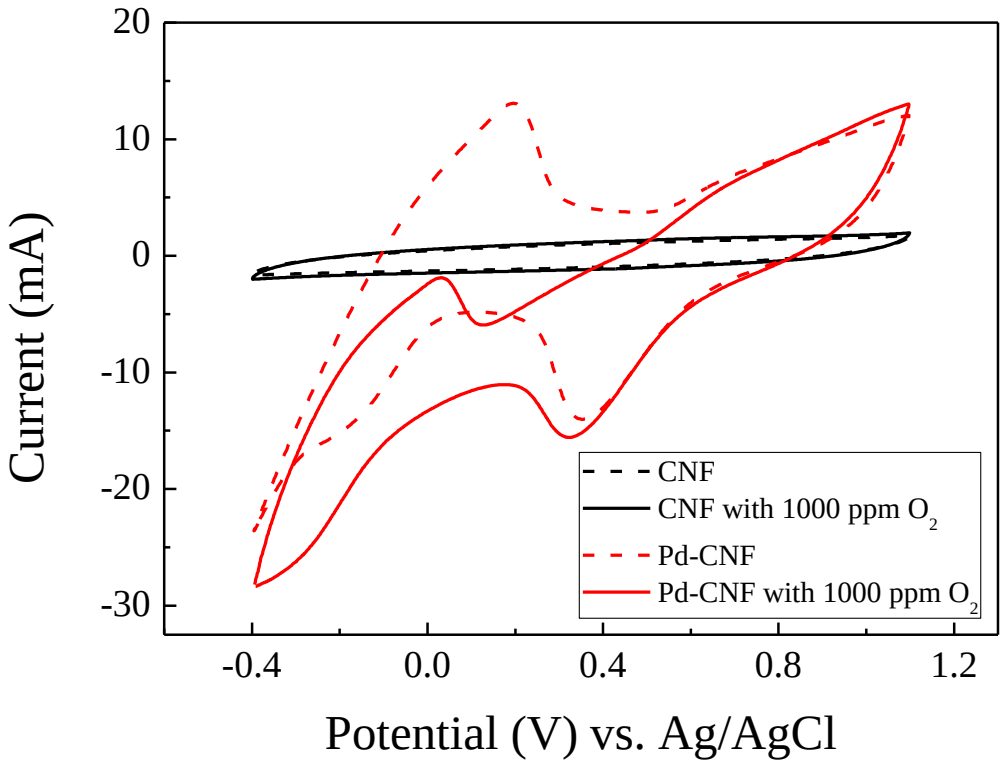

Figure 2. Cyclic voltammograms of the CNF and Pd-CNF electrodes in the presence and absence of 1000 ppm O_2 in 0.5 M $HClO_4$ solutions.

3.3 Determination of potential window

The polarization curves for the Pd-CNF electrode with and without 1000 ppm O_2 in 0.5 M $HClO_4$ solutions were shown in Fig. 3. In the absence of 1000 ppm O_2 (label as N_2), the background current of the Pd-CNF electrode increased from 0.001 to 7.22 mA when the applied potential was scanned from 0 to -0.3 V; this indicated proton absorption in this potential range.. In the presence of 1000 ppm O_2, the response current increased from 0.1 to 9.26 mA as the applied potential was scanned from 0.4 to -0.3 V. Fig. 3 also shows the net current of polarization curve calculated by the difference of Pd-CNF electrode with and without 1000 ppm O_2 . The response current increased from 0.04 to 3.45 mA as the applied potential was scanned from 0.4 to -0.2 V, and decreased to 1.73 mA when the applied potential was continued scanned to -0.4 V.Thus, an applied potential of -0.2 V was selected as the voltage for O_2 detection with the Pd-CNF electrode in 0.5 M $HClO_4$ solutions.

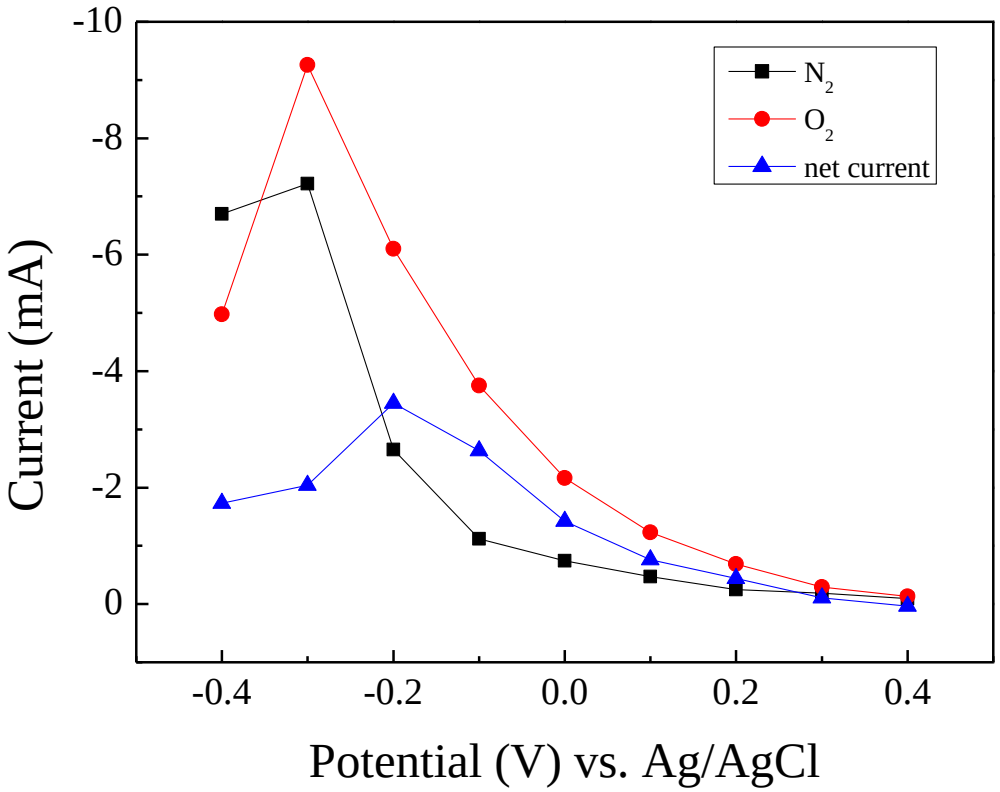

Figure 3. The polarization curves of the Pd-CNF electrode in the presence and absence of 1000 ppm O_2.

3.5. Amperometric Measurement

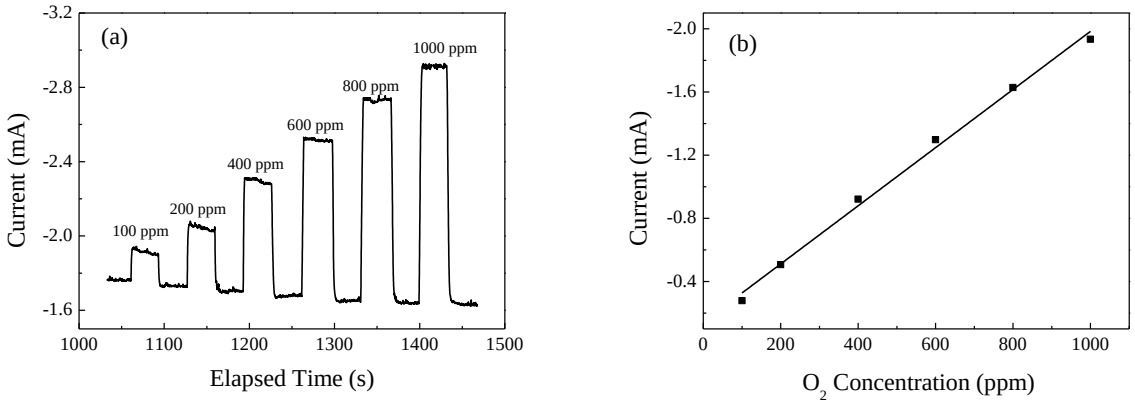

Figure 4. Amperometric responses of the Pd-CNF electrode in 0.5 M $HClO_4$ solutions at an applied potential of -0.2 V for various concentration of O_2 from 100 to 1000 ppm. Sensing conditions: applied potential, -0.2 V vs. Ag/AgCl; gas flow rate, 300 ml/min.

Figure 4(a) shows typical current-time responses of the Pd-CNF electrodes at an applied potential of -0.2 V in 0.5 M $HClO_4$ solutions. After obtaining a stable background current, O_2 was injected into the cell for increasing the O_2 concentration in the container from 0 to 100 ppm. The

cathodic current rose promptly until a stable value in the O_2 addition. After a certain time, the N_2 was again injected into the cell to purge the residual O_2. This procedure was repeated for measuring the current-time responses of the Pd-CNF electrodes at various O_2 concentrations of 200, 400, 600, 800 and 1000 ppm. Figure 4(b) plots the steady state values of the response currents versus different O_2 concentrations. The linear range was between 100 and 1000 ppm. The sensitivities of the Pd-CNF electrode was 2.34 $\mu Acm^{-2}ppm^{-1}$.

3.6 Response and Recovery Times

The effect of O_2 concentration on the response and recovery times of the Pd-CNF electrode is illustrated in Fig. 5. The response time is defined as the time required for the current increasing to 90% of its final value, measured from the onset of concentration change. The recovery time is defined as the time when the sensing current recovers to 90% of the background current. The response time of the Pd-CNF electrode is shorter than the recovery time. Both response and recovery times of the Pd-CNF electrode increase as the O_2 concentration increases. When the concentration was too high, many O_2 molecules penetrate the depth of sensing layers to react, which increases response time. The response and recovery times of sensor to O_2 are less than 32 and 48 s. In general, the electrode's pore volumes and active surface areas could strongly affect the response and recovery times of gas sensors [18-20]. The electrocatalysts with small pore volume and large active surface area lead to a fast response and a short recovery time. The Pd-CNF electrode exhibits short response and recovery times at room temperature, indicating that it possesses an optimal ratio of pore volumes to active surface areas.

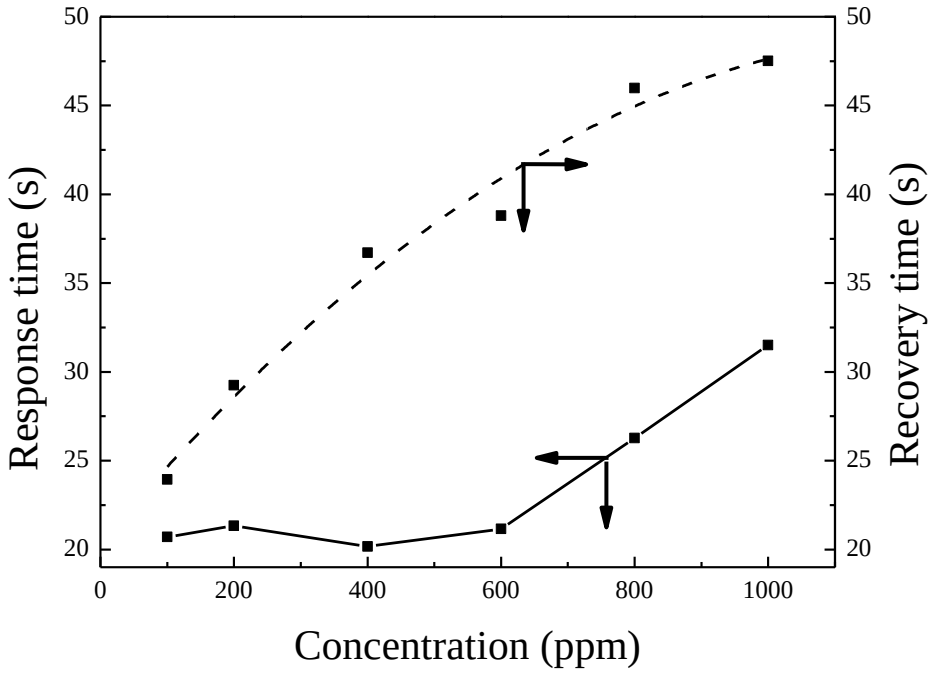

Figure 5. Response and recovery times for various concentration of O_2 on the Pd-CNF electrode.

3.7 Effect of Pd-CNF loading on Sensitivity

Fig. 6 shows the effect of the Pd-CNF loading on the sensitivity of the O_2 sensor. The sensitivity increased from 0.92 to 2.6 $\mu Appm^{-1}cm^{-2}$ by increasing the Pd-CNF loading from 1.8 to 4.7 mg, and the further increasing the Pd-CNF loading, the sensitivity decreased from 2.6 to 2.3 $\mu Appm^{-1}cm^{-2}$. The results showed that the sensitivity reached a maximum value 2.6 $\mu Appm^{-1}cm^{-2}$ at the Pd-CNF loading of 4.7 mg. The surface area of the Pd-CNF electrode increases with an increase in Pd-CNF loading. However, the electrodes become more compact and effective diffusivity decreases when the Pd-CNF loading increases.

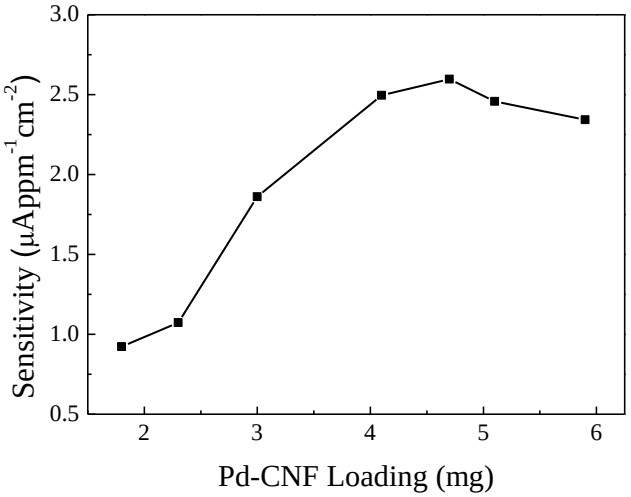

Figure 6. Effect of Pd-CNF loading on the sensitivity. Sensing conditions: applied potential, -0.2 V vs. Ag/AgCl; gas flow rate, 300 ml/min.

3.6 Interference Studies

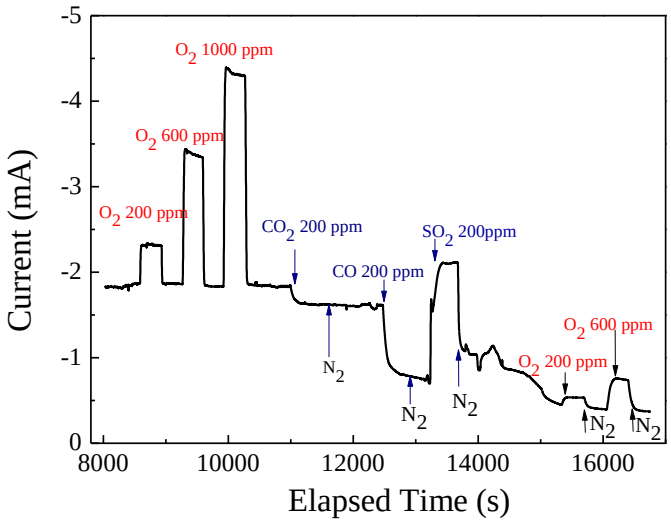

Figure 7. The selectivity of the Pd-CNF electrode for O_2, CO_2, CO and SO_2. Sensing conditions: applied potential, -0.2 V vs. Ag/AgCl; gas flow rate, 300 ml/min.

Table 1. Comparison of sensing performances for oxygen sensors with different modified electrodes.

Sensing materials	Applied potential	Range (ppm)	Response time (s)	Recovery time (s)	Sensitivity ($\mu A/cm^2$ ppm)	Ref.
Pt/Nafion Pd/Nafion	-0.15 V (vs. Ag/AgCl)	0-5000	60	_____	0.0538 0.0198	[18]
Au/Nafion®	-0.10 V (vs. Ag/AgCl)	100-1000	100	90	0.2676	[21]
Pt/Nafion	-0.2 V (vs. Ag/AgCl)	_____	58	_____	0.164	[22]
Cr /Pt/Nafion	0.148 V (vs. SHE)	1000-5000	142	147	0.533	[23]
Pd-CNF	-0.2 V (vs. Ag/AgCl)	100-1000	32	48	2.34	This work

The potential interfering species, such as CO_2, CO and SO_2 are used in this study. The interference test was performed at an applied potential of -0.2 V in a 0.5 M $HClO_4$ solution and evaluated by switching the gas between N_2 and a certain concentration of testing gas. Figure 7 displays the response current of the Pd-CNF electrode to the introduction and removal of testing gases. The continuous response-recovery current of the Pd-CNF electrode toward O_2, CO_2, CO, SO_2 and O_2 in sequence is recorded. When O_2 is injected to the system, the response current increases with the oxygen concentration increases. After N_2 is injected to the system, the response current quickly returns to the background current.

When the CO_2 is introduced, the response current decreases obviously, however, the current keeps constant even N_2 is injected to the system again. It suggests that CO_2 molecules adsorb on the surface of electrode and change the background current value. When CO is injected to the system, the response current drops again. The current stays constant after N_2 is injected to the system. It implies CO molecules also adsorb on the surface of electrode, changing the background current value. When SO_2 is injected to the system, the reduction current increases rapidly and the current declines when N_2 is injected to the system again. It indicates SO_2 molecules can be reduced on the surface of the electrode. When O_2 is injected to the system, the response current drops by 80% compared to fresh electrode, indicating that the electrode surface has been poisoned by interfering species. Thus, it is concluded that the Pd-CNF sensor is not specific for O_2 in the present of the SO_2 atmosphere. The selectivity may be improved by combination with selective pre-concentration schemes.

Table 1 displays the comparison of the amperometric oxygen sensors in literature [18, 21-23]. The Pd-CNF electrode has the highest sensitivity, fast response and recovery times for oxygen sensing when compared with other modified electrodes.

4. CONCLUSIONS

The Pd-CNF electrodes prepared by a two step procedure which consists of electrospinning and chemical reduction method were employed for oxygen detection. This sensor exhibits high sensitivity of 2.6 $\mu Appm^{-1}cm^{-2}$ to O_2 at room temperature. A linear relationship between sensing response with O_2 gas concentration has been demonstrated in the concentration range of 100 to 1000 ppm. The sensor also shows fast response and recovery times with the durations of less than 32 and 48 s, respectively.

ACKNOWLEDGEMENTS
Support from the Ministry of Science and Technology (MOST 106-2632-E-035-001-) and Feng Chia University is gratefully appreciated. The authors also appreciate the help of the Precision Instrument Support Center of Feng Chia University in providing the fabrication and measurement facilities. Appreciation is extended to Prof. Jia-Horng Lin and Prof. Chien-Lin Huang in the Department of Fiber and Composite Materials, Feng Chia University, for CNFs samples.

References

1. T.H. Tsai, C.Y. Yang, and S.M. Chen, *Int. J. Electrochem. Sci.*, 8 (2013**)** 5250.
2. J. Zhang, C. Zhao, P.A. Hu, Y.Q. Fu, Z.L. Wang, W.W. Cao, B. Yang and F. Placido, *RSC Adv.*, 3 (2013) 22185.
3. R. Baron, J. Saffell, *ACS Sens.,* 2 (2017) 1553.
4. C.O. Park, J.W. Fergus, N. Miura, J. Park and A. Choi, *Ionics*, 15 (2009) 261.
5. R. Knake, P. Jacquinot, A.W.E. Hodgson and P.C. Hauser, *Anal. Chim. Acta*, 549 (2005) 1.
6. B.J. Hwang, Y.C. Liu, and W.C. Hsu, *J. Solid State Electrochem.*, 2(1998) 378.
7. K. Wallgren, and S. Sotiropoulos, *Sens. Actuators, B*, 60 (1999) 174.
8. Y. Gao, H. Kita, Y. Watanabe and K. Sima. *J. Appl. Electrochem.*, 23 (1993) 1102.
9. R. Luoh, H.T. Hahn, *Compos. Sci. Technol.*, 66 (2006) 2436.
10. J.S. Huang, D.W. Wang, H.Q. Hou, T.Y. You, *Adv. Funct. Mater.*, 18 (2008) 441.
11. G. Sakai, N. Matsunaga, K. Shimanoe and N. Yamazoe, *Sens. Actuators, B*, 80 (2001) 125.
12. B.P.J.D Costello, R.J. Ewen, N. Guernion and N.M. Ratcliffe, *Sens. Actuators, B*, 87 (2002) 207.
13. S. Hrapovic, E. Majid, Y. Liu, K. Male and J.H.T. Luong, *Anal. Chem.*, 78 (2006) 5504.
14. W.Q. Yang, S.H. Yang, J.S. Guo, G.Q. Sun and Q. Xin, *Carbon*, 45 (2007) 397.
15. X.R. Ye, Y.H. Lin, C.M. Wang, M.H. Engelhard, Y. Wang and C.M. Wai, *J. Mater. Chem.*, 14 (2004) 908.
16. H. Zhu, M.L. Du, M. Zhang, M.L. Zou, T.T. Yang, L.N. Wang, J.M. Yao, B.C. Guo, *J. Mater. Chem. A*, 2 (2014) 11728.
17. H. Gabasch, W. Unterberger, K. Hayek, B. Klötzer, E. Kleimenov, D. Teschner, S. Zafeiratos, M. Hävecker, A. Knop-Gericke, R. Schlögl, J. Han, F.H. Ribeiro, B. Aszalos-Kiss, T. Curtin, D. Zemlyanov, *Surf. Sci.*, 600 **(**2006**)** 2980.
18. B.J. Hwang, Y.C. Liu and Y.L. Chen, *Mater. Chem. Phys.*, 69 (2001) 267.
19. B.J. Hwang, Y.C. Liu, and W.C. Hsu, *J. New Mater. Electrochem. Syst.*, 4 (2001) 69.
20. Y.C. Liu, B.J. Hwang, I. J. Tzeng, *J. Electrochem. Soc*., 149 (2002) 173.
21. B.J. Hwang, Y.C. Liu and W.C. Hsu, *J. Solid State Electrochem.*, 2 (1998) 378.
22. K. Wallgren, S. Sotiropoulos, *Sens. Actuators, B*, 60 (1999) 174.
23. Y.C. Liu, B.J. Hwang and I.J. Tzeng, *J. Electroanal. Chem.*, 533 (2002) 85.
24. A. Olean-Oliveira, and M.F.S. Teixeira, *Sens. Actuators, B*, 271 (2018) 353.
25. J. Luo, T. Dziubla, and R. Eitel, *Sens. Actuators, B*, 240 (2017) 392.

26. Y. Liu, Q. Wang, P. She, J. Gong, W.P. Wu, S.M. Xu, J.G. Li, K. Zhao, and A.P. Deng, *Microchim. Acta*, 183 (2016) 2847.